**Title:** USP7 Inhibition Promotes Early Osseointegration in Senile Osteoporotic mice

**Authors:** F Zhou[1,2], Z Wang[1,2], H Li[1,2], D Wang[1,2], Z Wu[1,2], F Bai[1,2], Q Wang[1], W Luo[1], G Zhang[1], Y Xiong[1,2], Y Wu[1,2*]

**Affiliations**：

1, State Key Laboratory of Oral Diseases, National Clinical Research Center for Oral Diseases, West China Hospital of Stomatology, Sichuan University, Chengdu, China

2, Department of Oral Implantology, West China Hospital of Stomatology, Sichuan University, Chengdu, China

***Correspondence should be addressed to:**

Yingying Wu, D.D.S, Ph.D.

State Key Laboratory of Oral Diseases, National Clinical Research Center for Oral Diseases, and Department of Oral Implantology, West China Hospital of Stomatology, Sichuan University, 14 Third Section, Renmin Nan Road, Chengdu 610041, China.

E-mail address: yywdentist@163.com

**Abstract Word Count: 249 words**

**Word Count (Introduction, Methods and Materials, Results and Discussion): 3193 words**

**Total Number of Tables/figures: 5 figures** in the main body of the manuscript, **7 figures,** and **2 tables** in the appendix

**Number of References: 36 references**

**Keywords:** senile osteoporosis, osseointegration, USP7, efferocytosis, senolysis

# USP7 Inhibition Promotes Early Osseointegration in Senile Osteoporotic mice

**Abstract:**

Although elderly osteoporotic patients have similar implant survival rates compared to those of normal individuals, they require longer healing periods to achieve proper osseointegration. This may be related to chronic inflammatory responses and impaired stem cell repair functions in the osteoporotic bone microenvironment. Recently, the deubiquitinating enzyme, USP7, was found to regulate macrophage immune response and modulate stem cell osteogenic differentiation. The selective inhibitor of USP7, P5091, has also been found to promote bone repair and homeostasis in osteoporotic conditions. However, the roles of USP7 and P5091 in osteoimmunology regulation and dental implant osseointegration under senile osteoporotic conditions remain unclear. In this study, USP7 depletion and P5091 were shown to inhibit inflammation in senescent bone marrow derived macrophages (BMDMs) and promote osteogenic differentiation in aged BMSCs. Furthermore, mRNA-Seq revealed that USP7 depletion could enhance efferocytosis in senescent BMDMs through the EPSIN1/LRP1 pathway and selectively induce apoptosis in aged BMSCs. In senile osteoporotic mice, we found that the osseointegration period was prolonged compared to young mice, and P5091 promoted the early stage of osseointegration, which may be related to macrophage efferocytosis around the implant. Collectively, this study suggests that USP7 inhibition may accelerate the osseointegration process in senile osteoporotic conditions by promoting macrophage efferocytosis and aged BMSCs apoptosis. This has implications for understanding the cellular interactions and signaling mechanisms in the peri-implant bone microenvironment under osteoporotic conditions. It may also provide clinical significance in developing new therapies to enhance osseointegration quality and shorten the edentulous period in elderly osteoporotic patients.

## INTRODUCTION

Senile osteoporosis, an age-related bone metabolic disease, leads to decreased bone quality, impaired bone healing, alveolar bone loss and tooth loss (Nicopoulou-Karayianni et al. 2009). The survival rates of dental implants in elder and osteoporotic patients do not differ significantly from those of normal individuals (Aghaloo et al. 2019; Srinivasan et al. 2017). However, osteoporotic patients exhibit poorer primary stability and more pronounced marginal bone loss (Lemos et al. 2023; Merheb et al. 2016). Consequently, osteoporotic patients often require longer time to achieve proper osseointegration (Tsolaki et al. 2009). Simultaneously, antiresorptive drugs such as bisphosphonates may increase the risk of medication-related osteonecrosis of the jaw (MRONJ) which is triggered by implant surgery (Jung et al. 2023; Sher et al. 2021). Therefore, researching new therapies to enhance osseointegration in senile osteoporotic patients has considerable clinical significance.

In a tibial implant model of aged mice, studies have found an excessive innate immune response in the peri-implant tissues of aged mice (Turajane et al. 2021). Overactive innate immune response in aged individuals can generate a chronic inflammatory microenvironment, which is called inflammaging (Ferrucci and Fabbri 2018). Inflammaging prolongs the inflammatory phase and impedes osteogenic differentiation of stem cells (Ma et al. 2023). Therefore, the interaction between macrophages and bone mesenchymal stem cells (BMSCs) plays a significant role in the early stage of osseointegration.

Ubiquitin-specific peptidase 7 (USP7) is a member of DUBs, which can cleave the ubiquitin chains from substrate proteins, thereby sparing them from degradation (Komander et al. 2009). Recently, Lin et al. found that P5091, a selective inhibitor targeting USP7, could inhibit osteoclast differentiation to alleviate bone loss in osteoporotic mice (Lin et al. 2023). On the contrary, Xie et al. found that USP7 inhibited osteoclast differentiation by stimulating STING, thereby reducing the level of bone loss in the skull (Xie et al. 2023). Therefore, USP7 may be an important therapeutic target for bone-related diseases. However, no studies have explored the role of USP7 in implant osseointegration.

In this study, we found that USP7 inhibition could selectively eliminated aged BMSCs and enhance the efferocytosis of senescent BMDMs via EPSIN1/LRP1 pathway. Moreover, through systemic injection of P5091, we found that USP7 inhibition could improve early stage of osseointegration in senile osteoporotic mice. Collectively, USP7 inhibition could enhance BMDMs efferocytosis and increase aged BMSCs apoptosis, which efficiently clear apoptotic senescent cell and inhibit macrophage inflammaging to promote early stage of osseointegration.

## Materials and Methods

Materials and methods were described in the Appendix Materials and Methods**.**

## Results

### Osseointegration is delayed in aged osteoporotic mice accompanied by elevated USP7 expression

In the femurs of male mice at 6, 12, and 18 months, MicroCT results showed that the 18-month-old mice exhibited a significant osteoporotic phenotype (Fig. 1A). Compared to the 6-month-old mice, the 18-month-old mice had significantly reduced bone volume and

trabecular bone thickness with increased trabecular bone separation in the cancellous bone (Fig. 1B). Additionally, the cortical bone thickness and area in the 18-month-old mice were also significantly decreased (Fig. 1C). Next, we used 6-month-old mice and 18-month-old mice as the young group and the aged group, and implanted titanium implants anterior to the first maxillary molar. We reconstructed the implant and the 200μm area surrounding the implant using MicroCT (Fig. 1D). The bone volume around the implants in aged mice consistently remained lower than that in young mice. However, both aged and young mice eventually achieved similar levels of bone-implant contact (BIC), while aged mice took 6 weeks to reach the BIC level that young mice achieved at 4-week. (Fig. 1E). These results indicated that aged mice had less bone volume around the implants and a slower rate of osseointegration. The differences in peri-implant bone volume and osseointegration level were most pronounced at 2-week and 4-week.

Next, we found that compared to aged mice, USP7 expression around the implants was overall lower in young mice. In aged mice, USP7 expression was significantly higher at 2-week, and became lower at 4-week (Fig. 1F). Through Western Blot (WB), we observed that USP7 expression was highest around the implants at 2-week in the aged group and significantly decreased at 4-week (Fig. 1G). This suggested that USP7 might play a significant role in the early stage of osseointegration in aged mice.

**USP7 is highly expressed in the aged BMSCs and senescent BMDMs**

We further investigated the expression changes of USP7 in BMSCs within aged mice. First, we found that USP7 and p16INK4a were minimally expressed in young BMSCs, whereas in aged BMSCs, both USP7 and p16INK4a were highly expressed in the cytoplasm and nucleus (Fig. 1H). WB also revealed that aged BMSCs expressed higher level of USP7 and p16INK4a significantly (Fig. 1I). This indicated that aged BMSCs exhibited a marked senescence state, accompanied by high USP7 expression. Next, we used conditioned media (CM) from aged BMSCs to treat BMDMs. BMDMs treated by CM of aged BMSCs had higher nuclear expression of p16INK4a, along with elevated USP7 expression (Fig. 1J). Similarly, WB results also showed that senescent BMDMs had a higher level of USP7 and p16INK4a expression (Fig. 1K).

**USP7 inhibition ameliorated inflammaging via NLRP3 pathway in senescent BMDMs**

Subsequently, we used CM from aged BMSCs to induce senescent BMDMs and conducted mRNA-Seq (Fig. 2A). USP7 was depleted by shRNA targeting USP7, which was evaluated by qPCR and WB (Fig. S1A-B). CCK8 assay showed that the cell viability of senescent BMDMs was lower than control BMDMs, while USP7 depletion did not alter it (Fig. S1C). KEGG

pathway enrichment analysis revealed that in USP7-depleted senescent BMDMs, the TNF-α, NFκB, Toll-like signaling pathway, and Nod-like receptor pathways were downregulated (Fig. 2B). GSEA also showed that NLRP3 pathway and innate immune response was significantly inhibited by USP7 depletion (Fig. 2C). Given previous studies reporting USP7's regulatory role on the NLRP3 pathway, we focused on the impact of USP7 on this pathway (Palazón-Riquelme et al. 2018). WB results showed that in senescent BMDMs, the protein level of p16INK4a was increased, accompanied by elevated levels of cleaved CASP1, GSDMD-NT, and cleaved IL-1β proteins. USP7 depletion significantly inhibited the expression of these proteins (Fig. 2D-E). Besides, we used P5091 to inhibit USP7. First, we screened the treatment concentration of P5091 using a CCK8 assay and found that 5μm of P5091 did not show significant cytotoxicity to BMDMs (Fig. S2A). Subsequently, we found that USP7 depletion and P5091 both significantly downregulated the mRNA levels and secretion of inflammatory cytokines such as IL-1β, IL-6, and TNF-α in senescent BMDMs (Fig. S1D-E; Fig. S2C-D).

**USP7 inhibition enhanced aged BMSCs osteogenesis co-cultured with BMDMs**

Next, we co-cultured USP7-depleted BMDMs with young/aged BMSCs. ALP/ARS staining indicated that USP7-depleted BMDMs significantly promoted osteogenesis in aged BMSCs (Fig. 2F). qPCR and WB results also indicated that USP7-depleted BMDMs significantly upregulated the mRNA and protein levels of osteogenic markers ALP, RUNX2, and COL1α1 in aged BMSCs (Fig. 2G-I). Regarding the senescence levels of aged BMSCs, SA-β-Gal staining indicated that USP7-depleted BMDMs significantly inhibited the senescence levels of aged BMSCs (Fig. 2J). Additionally, qPCR results suggested that USP7-depleted BMDMs inhibited the mRNA level of senescence-associated secretory phenotype (SASP) markers, *IL-1b* and *IL-6*, in aged BMSCs (Fig. 2K). Further, we used P5091 to inhibit USP7 in BMSCs co-cultured with BMDMs. We found that 5μm of P5091 did not show cytotoxicity to BMSCs like that of BMDMs (Fig. S2B). Therefore, we applied P5091 in the co-culture system. P5091 was found to improved osteogenesis by ALP/ARS staining (Fig. S2E). However, P5091 significantly inhibited COL1A1 expression in young BMSCs, while P5091 upregulated ALP, RUNX2, and COL1α1 in aged BMSCs (Fig. S2F). Regarding mRNA level, P5091 promoted osteogenic mRNA expression of *Alp, Runx2,* and *Col1a1* (Fig. S2G). The difference of mRNA and protein level of COL1α1 indicated that USP7 might played a post-transcriptional role in osteogenesis. Next, SA-β-Gal staining and qPCR also showed that P5091 also decreased the number of senescent cells and mRNA expression of *IL-1b*/*IL-6* in aged BMSCs co-cultured with BMDMs (Fig. S2H-I).

**USP7 inhibition promotes osteogenesis and senolysis of aged BMSCs**

Next, we investigated the effects of USP7 depletion and P5091 on BMSCs without BMDMs. We successfully depleted USP7 expression in BMSCs (Fig. S3A-B). USP7-depleted aged BMSCs exhibited a trend of suppressed SASP pathways, and promoted osteogenic differentiation and apoptotic pathways (Fig. 3A-B). Furthermore, CCK8 assay revealed that USP7 depletion inhibited cell viability of BMSCs significantly, while P5091 inhibited proliferation of aged BMSCs (Fig. 3C; Fig. S3C). Transwell migration assays further confirmed that USP7 depletion and P5091 promoted the migration of aged BMSCs (Fig. 3D; Fig. S3D). Regarding osteogenic capacity, ALP and ARS staining showed that USP7 depletion and P5091 enhanced osteogenesis of aged BMSCs, but P5091 inhibited osteogenesis of young BMSCs (Fig. 3E; Fig. S3E). WB indicated that USP7 depletion caused a significant reduction in the protein levels of ALP and COL1A1 in young BMSCs, while increasing these markers in aged BMSCs (Fig. 3F). P5091 significantly suppressed the expression of ALP and RUNX2 in young BMSCs, while substantially increasing the expression of osteogenic proteins in aged BMSCs (Fig. S3F). Additionally, USP7 depletion and P5091 significantly reduced the number of SA-β-gal-positive cells in aged BMSCs (Fig. 3G). USP7 depletion and P5091 also inhibited mRNA level and secretion level of IL-1β and IL-6 in aged BMSCs (Fig. 3H-I; Fig. S3H-I). Further, live-dead cell staining and flow cytometry revealed that USP7 depletion and P5091 promoted cell death in aged BMSCs without affecting young BMSCs (Fig. 3J-K; Fig. S3J-K)).

**USP7 inhibition orchestrates EPSIN1/LRP1 pathway to enhance efferocytosis**

Based on the mRNA-Seq results of USP7-depleted senescent BMDMs, KEGG pathway enrichment analysis revealed that the phagosome pathway was significantly upregulated in USP7-depleted senescent BMDMs (Fig. 4A). GSEA suggested that USP7 depletion upregulated efferocytosis capacity (apoptotic cell clearance) of senescent BMDMs (Fig. 4B). The heatmap of core genes showed that LRP1 expression was significantly upregulated in USP7-depleted senescent BMDMs (Fig. 4C). Studies have found that in macrophages, EPSIN1 could inhibit efferocytosis by promoting the ubiquitination and degradation of LRP1 (Brophy et al. 2019). Through WB, we found that ubiquitination level in senescent BMDMs was unchanged in different of groups of BMDMs, while EPSIN1 expression was increased and LRP1 expression was decreased. USP7 depletion downregulated EPSIN1 and upregulated LRP1 protein levels (Fig. 4D-E). Furthermore, after USP7 depletion, EPSIN1 protein levels gradually decreased over time, whereas overexpression of USP7 significantly delayed the degradation of EPSIN1 (Fig. S4A-B). Next, Co-IP experiments further validated the protein interaction between USP7 and EPSIN1 in BMDMs (Fig. 4F). Recombinant Flag-EPSIN1 and HA-USP7 proteins also demonstrated a similar interaction (Fig. S4C). By immunoprecipitating EPSIN1, Flag-EPSIN1, and ubiquitin, we found that USP7 depletion led to an increased ubiquitination level of EPSIN1 (Fig. 4G). Simultaneously, overexpression of HA-USP7 reduced the ubiquitination level of EPSIN1 without affecting the overall ubiquitination level (Fig. S4D-E).

This indicated that USP7 depletion might increase the ubiquitination level of EPSIN1, leading to its degradation, and LRP1 was spared from degradation, thereby promoting macrophage efferocytosis (Fig. S4F).

Subsequently, we inhibited LRP1-mediated efferocytosis in BMDMs by using the LRP1 inhibitor RAP and si*Lrp1*. RAP inhibited the mRNA levels of efferocytosis-related genes such as *Cd36, Mertk*, and *Lrp1* (Fig. S5A). We labeled apoptotic Jurkat cells and co-cultured them with BMDMs to evaluate efferocytosis efficiency. The results revealed that the efferocytosis ability of senescent BMDMs was significantly reduced, but USP7 depletion restored the efferocytosis capacity of senescent BMDMs (Fig. 4H-I). Additionally, USP7 depletion also enhanced the M2 polarization of senescent BMDMs after efferocytosis, while RAP inhibited this effect (Fig. S5B). qPCR results also showed that USP7 depletion inhibited the expression of pro-inflammatory genes and promoted the expression of anti-inflammatory genes in senescent BMDMs (Fig. S5C). Next, we co-cultured aged BMSCs and BMDMs. To avoid the impact of RAP on LRP1 in BMSCs, we transfected BMDMs with si*Lrp1*. The results showed that USP7-depleted senescent BMDMs promoted osteogenic differentiation in aged BMSCs, while depleting LRP1 in BMDMs weakened this pro-osteogenic effect (Fig. S5D).

**USP7 inhibition promoted early stage of osseointegration in aged mice via efferocytosis**

We further investigated the impact of USP7 inhibition on senile osteoporotic osseointegration in aged mice. P5091 treatment enhanced BIC and bone volume around implants in aged mice at 2-week and 4-week. The application of RAP attenuated the beneficial effect of P5091 on osseointegration (Fig. 5A-B). Similarly, HE staining indicated that aged mice treated with P5091 showed bone structure formation around the implants at 2-week, while Veh group and P50+RAP group showed no significant bone structure formation (Fig. S6A). Subsequently, we examined osteogenesis and osteoclastic activity around the implants using ALP and TRAP staining (Fig. 5C-D). ALP staining exhibited increased ALP expression in the peri-implant region of aged mice treated with P5091 compared to Veh and P50+RAP group at 2-week (Fig. 5E). Similarly, qPCR results revealed that bone tissue around implants expressed less osteogenic genes in aged mice compared to young mice, while P5091 upregulated both at 2-week and 4-week in aged mice (Fig. S6B). Regarding osteoclastic activity, TRAP staining showed that at 2-week, P5091 inhibited the number of osteoclasts around the implants in aged mice. At 4 weeks post-implantation, the number of osteoclasts around the implants in young mice were significantly reduced, whereas aged mice still maintained a relatively high level (Fig. 5F). Regarding immune response, pro-inflammatory cytokines, IL-1β and IL-6, were upregulated in aged mice, and P5091 inhibited these in aged mice at 2-week and 4-week. However, RAP abrogated the effect of P5091 on inhibiting inflammation (Fig. 5G). Subsequently, we employed TUNEL and F4/80 immunofluorescence staining to assess

changes in the number of apoptotic cells and the level of efferocytosis around the implants (Fig. 5H). At 2 weeks post-implantation, in young mice, P5091 did not significantly alter the number of apoptotic cells, macrophage counts, or efferocytosis levels. However, in aged mice, P5091 significantly increased the number of apoptotic cells and macrophages, and promoted efferocytosis. While the use of RAP did not alter the number of apoptotic cells, it significantly reduced the number of macrophages and suppressed efferocytosis (Fig. 5I). At 4 weeks post-implantation, both in young and aged mice, there were relatively fewer apoptotic cells and macrophages around the implants, and efferocytosis was also not evident (Fig. S7).

## DISCUSSION

In this study, to exclude the influence of estrogen levels on osteoporosis and related cellular behaviors, we used male mice aged 6 and 18 months. We found that senile osteoporosis resulted in significant delays in osseointegration and insufficient peri-implant bone volume. And during the early stage of osseointegration, there was an abnormally high expression of USP7 around the implants in aged mice. Recent studies observed that diabetic wound tissues exhibited a higher level of USP7 expression (Li et al. 2022; Zhang et al. 2024). P5091 could function as senolytic drug to eliminate senescent cells to reduce SASP, thereby mitigating overactivation of inflammation in diabetic wound. In aged individuals, early-stage osseointegration is characterized by impaired osteogenic differentiation and enhanced inflammatory response (Jiang et al. 2018; Turajane et al. 2021). Intrinsic aging of bone stem cells creates an inflammatory environment, which drives myeloid skewing and inflammation (Ambrosi et al. 2021). Accordingly, we found that CM from aged BMSCs upregulated p16INK4a and USP7 expression of BMDMs (defined as senescent BMDMs in this study). This suggested that USP7 played a crucial role in the early stage of osseointegration in aged mice and senescent BMSCs-BMDMs interaction. Inhibiting USP7 may help improve the function of aged BMSCs and senescent BMDMs.

Innate immune pathway and NLRP3 pathway were upregulated in the early stage of osseointegration (Chen et al. 2022). In this study, USP7 depletion and P5091 inhibited innate immune response and NLRP3 pathway in senescent BMDMs. Palazon et al. discovered that USP7 and USP47 directly maintained the NLRP3 pathway by preserving ASC speck formation (Palazón-Riquelme et al. 2018). Therefore, USP7-depleted BMDMs may exhibit a weaker inflammatory response when exposed to aging stimuli. Subsequently, we co-cultured BMDMs with BMSCs, and found that the osteogenic capacity of aged BMSCs co-cultured with USP7-depleted BMDMs was rescued. Adding P5091 to the co-culture system similarly promoted osteogenic differentiation of aged BMSCs. Li and colleagues discovered that in the bone marrow of aged mice, 80% of macrophages exhibit the M1 phenotype (whereas in young

mice, M1 macrophages only make up 5%) (Li et al. 2021). M1 to M2 polarization induced-immunomodulation is vital for BMSCs osteogenesis and successful osseointegration (Ma et al. 2018; Wang et al. 2022). As a result, USP7 inhibition might inhibit inflammaging of senescent BMDMs, thereby improve osteogenesis of aged BMSCs.

Further, we observed that USP7 depletion, inhibited cell viability of BMSCs, which also while increasing osteogenic capacity in aged BMSCs, led to a reduction of ALP and COL1A1 in young BMSCs. Similarly, Kim et al. demonstrated that after USP7 depletion, the ubiquitination levels of NANOG and SOX2 increased, subsequently inhibiting self-renewal capacity and multipotency of BMSCs (Kim et al. 2022). Consequently, USP7 plays a different role between young and aged BMSCs. In this study, we discovered that USP7 depletion promoted apoptosis and osteoblast differentiation in aged BMSCs, while SASP pathway was inhibited. P5091 were found as a senolytic drug to selectively kill senescent cells (He et al. 2020). Farr et al. utilized dasatinib and quercetin, a classic senolytic therapy, to eliminate senescent cells in aged mice and alleviate of osteoporosis (Farr et al. 2017). Baima et al. proposed that periodontitis, as an age-related disease, might be potentially treatable with senotherapy targeting MSCs (Baima et al. 2022). Therefore, senolytic therapies in aged BMSCs may also promote osseointegration in aged individuals.

Phagocytosis of apoptotic cells is a crucial process for macrophages to transition from the M1 phase during the wound inflammation stage to the M2 phase during the wound proliferation stage, which is also known as efferocytosis (Gerlach et al. 2021). In aging individuals, macrophages may experience impaired efferocytosis functions because of impaired MerTK function (Rymut et al. 2020). This may lead to ineffective clearance of apoptotic cells in the early stage of osseointegration, and macrophages may struggle to transition into the M2 phenotype. In this study, we observed that USP7 depletion improved the impaired efferocytosis via upregulation of LRP1 in senescent BMDMs. LRP1 is a key receptor involved in mediating efferocytosis (Doddapattar et al. 2022). LRP1 was found to play a vital role in bone metabolism (Lu et al. 2018). We validated that USP7 could orchestrate efferocytosis in senescent BMDMs via EPSIN/LRP1 pathway, and targeting LRP1 could abrogate pro-osteogenic capacity of senescent BMDMs.

In the *in vivo* experiments, since knockout of USP7 might lead to embryonic lethality, and tamoxifen required for CreERT2 can affect bone metabolism, we therefore used P5091 to inhibit USP7 in mice (Chen et al. 2023; Kon et al. 2010). We calculated apoptotic cell-associated macrophages by labeling apoptotic cells with TUNEL and labeling macrophages with F4/80 as former studies (Gerlach et al. 2021; Shi et al. 2022). P5091

improved early stage of osseointegration of senile osteoporotic mice via efferocytosis. In periodontitis, promoting macrophage efferocytosis mediated by DEL-1 has been shown to alleviate periodontal inflammation and reduce alveolar bone resorption (Kourtzelis et al. 2019). Simultaneously, we found that P5091 inhibited pro-inflammatory cytokines in peri-implant region which was overactivated in aged mice. Inhibiting efferocytosis via RAP upregulated inflammatory response in aged mice. Therefore, therapies targeting efferocytosis may improve senile osteoporotic osseointegration, which was related to reduced immune response mediated by efferocytosis.

## References


Aghaloo T, Pi-Anfruns J, Moshaverinia A, Sim D, Grogan T, Hadaya D. 2019. The effects of systemic diseases and medications on implant osseointegration: A systematic review. Int J Oral Maxillofac Implants. 34:s35-s49.

Ambrosi TH, Marecic O, McArdle A, Sinha R, Gulati GS, Tong X, Wang Y, Steininger HM, Hoover MY, Koepke LS et al. 2021. Aged skeletal stem cells generate an inflammatory degenerative niche. Nature. 597(7875):256-262.

Baima G, Romandini M, Citterio F, Romano F, Aimetti M. 2022. Periodontitis and accelerated biological aging: A geroscience approach. J Dent Res. 101(2):125-132.

Brophy ML, Dong Y, Tao H, Yancey PG, Song K, Zhang K, Wen A, Wu H, Lee Y, Malovichko MV et al. 2019. Myeloid-specific deletion of epsins 1 and 2 reduces atherosclerosis by preventing lrp-1 downregulation. Circ Res. 124(4).

Chen M-Y, Zhao F-L, Chu W-L, Bai M-R, Zhang D-M. 2023. A review of tamoxifen administration regimen optimization for cre/loxp system in mouse bone study. Biomed Pharmacother. 165:115045.

Chen Y, Li J, Shi J, Ning D, Feng J, Lin W, He F, Xie Z. 2022. Ipriflavone suppresses nlrp3 inflammasome activation in host response to biomaterials and promotes early bone healing. J Clin Periodontol. 49(8):814-827.

Doddapattar P, Dev R, Ghatge M, Patel RB, Jain M, Dhanesha N, Lentz SR, Chauhan AK. 2022. Myeloid cell pkm2 deletion enhances efferocytosis and reduces atherosclerosis. Circ Res. 130(9):1289-1305.

Farr JN, Xu M, Weivoda MM, Monroe DG, Fraser DG, Onken JL, Negley BA, Sfeir JG, Ogrodnik MB, Hachfeld CM et al. 2017. Targeting cellular senescence prevents age-related bone loss in mice. Nat Med. 23(9):1072-1079.

Ferrucci L, Fabbri E. 2018. Inflammageing: Chronic inflammation in ageing, cardiovascular disease, and frailty. Nat Rev Cardiol. 15(9):505-522.

Gerlach BD, Ampomah PB, Yurdagul A, Liu C, Lauring MC, Wang X, Kasikara C, Kong N, Shi J, Tao W et al. 2021. Efferocytosis induces macrophage proliferation to help resolve tissue injury. Cell metabolism. 33(12).

He Y, Li W, Lv D, Zhang X, Zhang X, Ortiz YT, Budamagunta V, Campisi J, Zheng G, Zhou D. 2020. Inhibition of usp7 activity selectively eliminates senescent cells in part via restoration of p53 activity. Aging cell. 19(3):e13117.

Jiang L, Zhang W, Wei L, Zhou Q, Yang G, Qian N, Tang Y, Gao Y, Jiang X. 2018. Early effects of parathyroid hormone on vascularized bone regeneration and implant osseointegration in aged rats. Biomaterials. 179:15-28.

Jung J, Ryu J-I, Shim G-J, Kwon Y-D. 2023. Effect of agents affecting bone homeostasis on short- and long-term implant failure. Clin Oral Implants Res. 34 Suppl 26:143-168.

Kim YJ, Park KH, Lee K-M, Chun Y-M, Lee JW. 2022. Deubiquitinating enzyme usp7 is required for self-renewal and multipotency of human bone marrow-derived mesenchymal stromal cells. International journal of molecular sciences. 23(15).

Komander D, Clague MJ, Urbé S. 2009. Breaking the chains: Structure and function of the deubiquitinases. Nat Rev Mol Cell Biol. 10(8):550-563.

Kon N, Kobayashi Y, Li M, Brooks CL, Ludwig T, Gu W. 2010. Inactivation of hausp in vivo modulates p53 function. Oncogene. 29(9):1270-1279.

Kourtzelis I, Li X, Mitroulis I, Grosser D, Kajikawa T, Wang B, Grzybek M, von Renesse J, Czogalla A, Troullinaki M et al. 2019. Del-1 promotes macrophage efferocytosis and clearance of inflammation. Nat Immunol. 20(1):40-49.

Lemos CAA, de Oliveira AS, Faé DS, Oliveira HFFE, Del Rei Daltro Rosa CD, Bento VAA, Verri FR, Pellizzer EP. 2023. Do dental implants placed in patients with osteoporosis have higher risks of failure and marginal bone loss compared to those in healthy patients? A systematic review with meta-analysis. Clin Oral Investig. 27(6):2483-2493.

Li C-J, Xiao Y, Sun Y-C, He W-Z, Liu L, Huang M, He C, Huang M, Chen K-X, Hou J et al. 2021. Senescent immune cells release grancalcin to promote skeletal aging. Cell metabolism. 33(10).

Li X, Wang T, Tao Y, Wang X, Li L, Liu J. 2022. Inhibition of usp7 suppresses advanced glycation end-induced cell cycle arrest and senescence of human umbilical vein endothelial cells through ubiquitination of p53. Acta Biochim Biophys Sin (Shanghai). 54(3):311-320.

Lin Y-C, Zheng G, Liu H-T, Wang P, Yuan W-Q, Zhang Y-H, Peng X-S, Li G-J, Wu Y-F, Shen H-Y. 2023. Usp7 promotes the osteoclast differentiation of cd14+ human peripheral blood monocytes in osteoporosis via hmgb1 deubiquitination. J Orthop Translat. 40:80-91.

Lu D, Li J, Liu H, Foxa GE, Weaver K, Li J, Williams BO, Yang T. 2018. Lrp1 suppresses bone resorption in mice by inhibiting the rankl-stimulated nf-κb and p38 pathways during osteoclastogenesis. J Bone Miner Res. 33(10):1773-1784.

Ma Q-L, Fang L, Jiang N, Zhang L, Wang Y, Zhang Y-M, Chen L-H. 2018. Bone mesenchymal stem cell secretion of srankl/opg/m-csf in response to macrophage-mediated inflammatory response influences osteogenesis on nanostructured ti surfaces. Biomaterials. 154:234-247.

Ma Y, Wang S, Wang H, Chen X, Shuai Y, Wang H, Mao Y, He F. 2023. Mesenchymal stem cells and dental implant osseointegration during aging: From mechanisms to therapy. Stem cell research & therapy. 14(1):382.

Merheb J, Temmerman A, Rasmusson L, Kübler A, Thor A, Quirynen M. 2016. Influence of skeletal and local bone density on dental implant stability in patients with osteoporosis. Clin Implant Dent Relat Res. 18(2):253-260.

Nicopoulou-Karayianni K, Tzoutzoukos P, Mitsea A, Karayiannis A, Tsiklakis K, Jacobs R, Lindh C, van der Stelt P, Allen P, Graham J et al. 2009. Tooth loss and osteoporosis: The osteodent study. J Clin Periodontol. 36(3):190-197.

Palazón-Riquelme P, Worboys JD, Green J, Valera A, Martín-Sánchez F, Pellegrini C, Brough D, López-Castejón G. 2018. Usp7 and usp47 deubiquitinases regulate nlrp3 inflammasome activation. EMBO reports. 19(10).

Rymut N, Heinz J, Sadhu S, Hosseini Z, Riley CO, Marinello M, Maloney J, MacNamara KC, Spite M, Fredman G. 2020. Resolvin d1 promotes efferocytosis in aging by limiting senescent cell-induced mertk cleavage. FASEB journal : official publication of the Federation of American Societies for Experimental Biology. 34(1):597-609.

Sher J, Kirkham-Ali K, Luo JD, Miller C, Sharma D. 2021. Dental implant placement in patients with a history of medications related to osteonecrosis of the jaws: A systematic review. J Oral Implantol. 47(3):249-268.

Shi J, Wu X, Wang Z, Li F, Meng Y, Moore RM, Cui J, Xue C, Croce KR, Yurdagul A et al. 2022. A genome-wide crispr screen identifies wdfy3 as a regulator of macrophage efferocytosis. Nature communications. 13(1):7929.

Srinivasan M, Meyer S, Mombelli A, Müller F. 2017. Dental implants in the elderly population: A systematic review and meta-analysis. Clin Oral Implants Res. 28(8):920-930.

Tsolaki IN, Madianos PN, Vrotsos JA. 2009. Outcomes of dental implants in osteoporotic patients. A literature review. J Prosthodont. 18(4):309-323.

Turajane K, Ji G, Chinenov Y, Chao M, Ayturk U, Suhardi VJ, Greenblatt MB, Ivashkiv LB, Bostrom MP, Yang X. 2021. Rna-seq analysis of peri-implant tissue shows differences in immune, notch, wnt, and angiogenesis pathways in aged versus young mice. JBMR Plus. 5(11):e10535.

Wang Y, Wang J, Gao R, Liu X, Feng Z, Zhang C, Huang P, Dong A, Kong D, Wang W. 2022. Biomimetic glycopeptide hydrogel coated pcl/nha scaffold for enhanced cranial bone regeneration via macrophage m2 polarization-induced osteo-immunomodulation. Biomaterials. 285:121538.

Xie Z, Wu Y, Shen Y, Guo J, Yuan P, Ma Q, Wang S, Jie Z, Zhou H, Fan S et al. 2023. Usp7 inhibits osteoclastogenesis via dual effects of attenuating traf6/tak1 axis and stimulating sting signaling. Aging Dis. 14(6):2267-2283.

Zhang S, Meng N, Liu S, Ruan J, Li H, Xu X, Ruan Q, Xie W. 2024. Targeting senescent hdf with the usp7 inhibitor p5091 to enhance dfu wound healing through the p53 pathway. Biochemical and biophysical research communications. 722:150149.

## Author Contributions

F. Zhou, contributed to conception, methodology, validation, formal analysis, investigation, resources, data curation, and drafted the manuscript; Z. Wang, H Li, D. Wang, contributed to investigation, methodology ,data curation; Z. Wu, B. F, contributed to original draft, formal analysis, visualization; Q. Wang, W. Luo, G. Zhang, contributed to original draft ;Y. Xiong, contributed to data interpretation and critically revised the manuscript; Y. Wu, contributed to project administration, supervision, and critically revised the manuscript. All authors gave their final approval and agree to be accountable for all aspects of the work.

## Declaration of Conflicting Interests

The authors declared no potential conflicts of interest with respect to the research, authorship, and/or publication of this article.

**Acknowledgement**

We acknowledge the funding from the National Natural Science Foundation of China (81970966, 82001084), Natural Science Foundation of Sichuan Province (2023NSFSC1513, 2023NSFSC0574).

**Data and materials availability**

All data are available in the main text or the supplementary materials upon reasonable requests

**Fig. 1 Senile osteoporotic mice exhibited a delayed osseointegration and higher expression of USP7.**

Different age of male mice (6-month, 12-month and 18-month) were employed. (A) Three-dimensional reconstruction image of cancellous and cortical bone in femurs at the position 700μm below the growth plate, scale bar, 500μm. (B) Quantitative MicroCT analysis of cancellous bone, n = 5. (C) Quantitative MicroCT analysis of cortical bone, n = 5. (D) Three-dimensional reconstruction image of alveolar bone around implants after 2 weeks and 4 weeks, scale bar, 600μm. (E) Quantitative MicroCT analysis of the 200μm region around the implants. (F) Immunohistochemical staining of USP7 around the implant, scale bar, 100μm. (G) Western blot analysis and quantification of USP7 expression in the bone tissue around implants, n = 3. (H) Immunofluorescence staining of USP7, p16INK4a, and DAPI in young and aged BMSCs. (I) Western blot analysis and quantification of USP7 and p16INK4a expression in the BMSCs, n = 3. (I) Immunofluorescence staining of USP7, p16INK4a, and DAPI in control and senescent BMDMs. (J) (K) Western blot analysis and quantification of USP7 and p16INK4a expression in the BMDMs, n = 3. BV/TV, bone volume per tissue volume; Tb.N, trabecular number; Tb.Th, trabecular thickness; Tb.Sp, trabecular separation; Ct.Th, cortical bone thickness; Ct.Ar, cortical bone area; BIC, bone-implant intact; Young, young BMSCs; Aged, aged BMSCs; CON, control BMDMs; SEN, senescent BMDMs . Data are shown as the mean ± SD; ns, not significant, *$P < 0.05$, **$P < 0.01$, ***$P < 0.001$, ****$P < 0.0001$.

**Fig. 2 USP7 depletion inhibited inflammaging in senescent BMDMs and promoted osteogenesis of aged BMSCs co-cultured with BMDMs**

(A) schematic diagram showing the induction of senescent BMDMs and mRNA-Seq analysis. (B) KEGG pathway enrichment analysis of senescent and USP7-depleted senescent BMDMs. (C) GSEA showing decreased enrichment of innate immune response pathway-associated

genes and Nod-like receptor (NLR) signaling pathway-associated genes in USP7-depleted senescent BMDMs. (D) Western blot analysis and (E) quantification of p16INK4a, cleaved caspase-1, GSDMD-NT, and cleaved IL-1β in different groups of BMDMs, n = 3. (F) Representative images of ALP and ARS staining in young/aged BMSCs co-cultured with different groups of BMDMs for 7d and 14d. (G) qPCR analyses of the mRNA levels of *Alp*, *Runx2*, *Col1a1* in young/aged BMSCs co-cultured with BMDMs for 7d, n = 3. (H) Western blot analysis and (I) quantification of ALP, RUNX2, and COL1α1 in young/aged BMSCs co-cultured with different groups of BMDMs for 7d, n = 3. (J) Representative images of SA-β-gal staining of young/aged BMSCs co-cultured with different groups of BMDMs for 3d, scale bar, 50μm. (K) qPCR results of *IL-1b* and *IL-6* in young/aged BMSCs co-cultured with different groups of BMDMs for 3d, n = 3. Y-BMSCs, young BMSCs; A-BMSCs, aged BMSCs; shNC, BMDMs transfected with NC lentivirus; sh*Usp7*, BMDMs transfected with sh*Usp7* lentivirus; CON, control BMDMs; SEN, senescent BMDMs; Upper, upper well of transwell system; Lower, lower well of transwell system. Data are shown as the mean ± SD; ns, not significant, **P* < 0.05, ***P* < 0.01, ****P* < 0.001, *****P* < 0.0001.

**Fig. 3 USP7 depletion promoted osteogenesis and senolysis in aged BMSCs**

(A) schematic diagram showing mRNA-Seq analysis of young and aged BMSCs treated with shNC or sh*Usp7*. (B) GSEA showing decreased enrichment of SASP pathway-associated genes and elevated enrichment of osteoblast differentiation and apoptosis pathway-associated genes in USP7-depleted aged BMSCs. (C) CCK8 assay for determining cell viability of young/aged BMSCs transfected with shNC or sh*Usp7* lentivirus at 3d, n=5. (D) Representative images and quantitative analysis of migration capacity of young/aged BMSCs for 24 h, n = 3, scale bar, 50μm. (E) Representative images of ALP and ARS staining in different groups of BMSCs after initiating osteogenic induction for 7 and 14 d. (F) Western blot and quantification of ALP, RUNX2, and COL1α1 in different group of BMSCs after initiating osteogenic induction for 7 d, n = 3. (G) Representative images of SA-β-gal staining of different BMSCs, scale bar, 50μm. (H) qPCR results and (I) ELISA results of IL-1β and IL-6 in different groups of BMSCs, n = 3. (J) Representative images of live/dead staining of BMSCs after transfected with shNC or shUsp7 lentivirus for 3d, green color indicates live cells, red color indicates dead cells, scale bar, 150μm. (K) Flow cytometry and quantification for apoptosis in BMSCs after transfected with shNC or shUsp7 lentivirus for 3d. shNC, BMSCs transfected with shNC lentivirus; sh*Usp7*, BMSCs transfected with sh*Usp7* lentivirus. Data are shown as the mean ± SD; ns, not significant, **P* < 0.05, ***P* < 0.01, ****P* < 0.001, *****P* < 0.0001.

**Fig. 4 USP7 depletion promoted efferocytosis capacity in senescent BMDMs via EPSIN1/LRP1 pathway**

(A) KEGG pathway enrichment analysis indicated an upregulated phagosome pathway in USP7-depleted senescent BMDMs. (B) GSEA showing elevated enrichment of apoptotic cell clearance pathway-associated genes. (C) Heatmap of representative apoptotic cell clearance-related genes in senescence and USP7-depleted senescent BMDMs. (D) Western blot and (E) quantification of ubiquitin, USP7, EPSIN1, and LRP1 in different group of BMDMs, n = 3. (F) Co-IP detecting the interaction between USP7 and EPSIN1. (G) Co-IP detecting the ubiquitous level of EPSIN1 in BMDMs transfected with shNC or sh*Usp7*. (H) Representative images and quantification of efferocytosis ratio of control/senescent BMDMs co-cultured with calcein-labeled apoptotic Jurkat cells for 24 h, n = 3, scale bar, 150μm. (I) Flow cytometry analysis for evaluating efferocytosis capacity of control/senescent BMDMs co-cultured with DiIC18(5)-DS-labeled apoptotic Jurkat cells for 24 h. DiIC18(5)-DS-positive and F4/80-postive cells indicated apoptotic cell-associated macrophages, n = 3. shNC, BMDMs transfected with NC lentivirus; sh*Usp7*, BMDMs transfected with sh*Usp7* lentivirus; CON, control BMDMs; SEN, senescent BMDMs; HC, heavy chain of IgG. Data are shown as the mean ± SD; ns, not significant, **P* < 0.05, ***P* < 0.01, ****P* < 0.001, *****P* < 0.0001.

**Fig. 5 P5091 improved early stage of osseointegration in senile osteoporotic mice via efferocytosis**

(A) Representative three-dimensional reconstruction images of alveolar bone around implants, scale bar. 600μm. (B) Quantitative MicroCT analysis of the 200μm region around the implants, n = 6. (C) Immunohistochemical staining of ALP around the implant, scale bar, 100μm. (D) TRAP staining around the implant, scale bar, 100μm. (E) Quantification of ALP-positive area in bone tissue around implants, n = 5. (F) Quantification of TRAP-positive osteoclasts in bone tissue around implants, n = 5. (G) qPCR results of *IL-1b* and *IL-6* expression in the bone tissue around implants, n = 4. (H) Representative immunofluorescence images of macrophages and apoptotic cells around the implants, and white arrows indicated the apoptotic cells engulfed by macrophages, scale bar, 100μm. (I) Quantification of apoptotic cell number, F4/80-positive macrophage number and efferocytosis efficiency (efferocytotic macrophages were determined as apoptotic cell-associated macrophages), n = 5. Veh, mice treated with vehicle (DMSO); P5091, mice treated with P5091; P50+RAP, mice treated with P5091 and RAP; Y, young mice; A, aged mice. Data are shown as the mean ± SD; ns, not significant, **P* < 0.05, ***P* < 0.01, ****P* < 0.001, *****P* < 0.0001.

**Supplementary File**

**Title:** USP7 Inhibition Promotes Early Osseointegration in Senile Osteoporotic mice

**Authors:** F Zhou[1,2], Z Wang[1,2], H Li[1,2], D Wang[1,2], Z Wu[1,2], F Bai[1,2], Q Wang[1], W Luo[1], G Zhang[1], Y Xiong[1,2], Y Wu[1,2,*]

**Affiliations**：

1, State Key Laboratory of Oral Diseases, National Clinical Research Center for Oral Diseases, West China Hospital of Stomatology, Sichuan University, Chengdu, China

2, Department of Oral Implantology, West China Hospital of Stomatology, Sichuan University, Chengdu, China

***Correspondence should be addressed to:**

Yingying Wu, D.D.S, Ph.D.

State Key Laboratory of Oral Diseases, National Clinical Research Center for Oral Diseases, and Department of Oral Implantology, West China Hospital of Stomatology, Sichuan University, 14 Third Section, Renmin Nan Road, Chengdu 610041, China.

E-mail address: yywdentist@163.com

## Appendix Materials and Methods

### In vitro experiments

#### Cell culture and co-culture of BMSCs-BMDMs

Young and aged BMSCs were extracted from 6-month and 18-month mice, which were cultured in the growth medium consisting of DMEM (Gibco), supplemented with 10% FBS (Gibco), and 1% penicillin and streptomycin. BMDMs were extracted from 6-month mice, and plated in pre-cooled prepared bone marrow macrophage differentiation medium containing DMEM (Gibco), 10% FBS (Gibco), 1% penicillin/streptomycin, and 20 ng/mL monocyte-colony stimulating factor (M-CSF, PeproTech). When inducing senescent BMDMs, conditional media (CM) from aged BMSCs was used to culture BMDMs. CM from aged BMSCs was mixed with macrophage differentiation medium in a 1:3 ratio. To inhibit USP7 and LRP1 in cells, P5091 (MCE) was dissolved in DMSO and applied in BMSCs and BMDMs at the concentration of 5μM, while receptor-associated protein (RAP, Abcam) was dissolved in PBS and applied in BMDMs at the concentration of 150nM.

As for the co-culture of BMSCs-BMDMs, in the indirect co-culture system, 0.4 μm 24-well Transwell inserts were utilized to co-culture BMSCs and BMDMs. For the direct co-culture system, a 24-well plate was used to co-culture BMSCs and BMDMs. A total of 60,000 BMSCs and 60,000 BMDMs were simultaneously seeded into the 24-well plate, and 500 μL of growth medium containing 20 ng/mL M-CSF was added.

#### Transfection of BMSCs and BMDMs

BMDMs and BMSCs were transfected with a lentiviral psi-LVRU6P vector expressing Usp7 shRNA or control shNC (shNegativeControl, GeneCopoeia). When BMSCs or BMDMs

reached approximately 70-90% confluence, they were subjected to transfection at multiplicity of infection (MOI) of 50 with polybrene (5 mg/mL, Sigma). The transfection process took place at 37°C in a 5% CO2 environment for 24 hours. Subsequently, the supernatant was removed, and normal growth medium was added. After 2 days, puromycin (Sigma) was used to select shRNA-induced cells. As for siRNA transfection, si*Lrp1* (GeneCopoeia) was transfected to BMDMs with application of EndoFectin Max (GeneCopoeia). After 18h, BMDMs were rinsed by PBS and cultured with complete medium for 48h. Then BMDMs transfected with si*Lrp1* were used for subsequent experiments.

**mRNA-seq**

The transcriptome sequencing and subsequent analysis were conducted by OE Biotech Co., Ltd. (Shanghai, China). Briefly, total RNAs were extracted utilizing the TRizol reagent (Invitrogen). The purity and concentration of the RNA were determined with a NanoDrop 2000 spectrophotometer (Thermo Scientific). Subsequently, libraries were prepared in accordance with the manufacturer's protocol using the VAHTS Universal V6 RNA-seq Library Prep Kit. The libraries were subjected to sequencing on an Illumina Novaseq 6000 platform, yielding 150 bp paired-end reads. Quality control of the mRNA-seq data was carried out using FastQC (v0.11.5) and the FASTX toolkit (0.0.13). Alignment to the Mus musculus reference genomes was performed using HISAT2 (v.2.0.4). Differentially expressed genes between shUsp7 and shNC groups were identified using the DEseq2 package (version 1.34.0) if they met the criteria of Q value < 0.05 and a fold change greater than 2 or less than 0.5.

**Cell proliferation assay**

The cell proliferation of BMSCs and BMDMs was evaluated using Cell Counting Kit-8 (CCK-8,

Beyotime) assay. A mixture containing 100 μL of 10% CCK-8 assay reagent was added to each well. Following incubation in the absence of light for 1.5 hours, the optical density (OD) was determined at 450 nm using a Varioskan Flash microplate reader (Thermo Scientific).

**Migration assay**

BMSCs were initially plated at a density of $2 \times 10^4$ cells per well in 24-transwell plates (Corning). Following a 24-hour incubation period, BMSCs present in the transwell chambers were fixed for 30 minutes by 4% paraformaldehyde (Biosharp), stained with 0.1% w/v crystal violet (Beyotime) for an additional 45 minutes, and subsequently visualized using an inverted microscope (Leica).

**RNA extraction and quantificational real-time PCR (qRT-PCR)**

Total RNA was extracted from the alveolar bone tissue around implants and treated BMSCs/BMDMs following the manufacturer's guidelines, employing a total RNA isolation kit from Vazyme. Bone tissue around implants was first separated from maxilla and immersed in liquid nitrogen, which were were ground into a paste using a mortar and pestle. Subsequently, RNA samples underwent reverse transcription into cDNA utilizing the HiScript® III All-in-one RT SuperMix, ideally suited for qPCR (Vazyme). Quantitative real-time polymerase chain reaction (qRT-PCR) was carried out using Taq Pro Universal SYBR qPCR Master Mix (Vazyme). A list of the primers employed is provided in Supplementary Table 1. The relative gene expression levels were determined using the $2^{-\Delta\Delta}$CT method, normalizing to β-actin as the internal reference gene.

**Western blot**

The cell protein of treated BMDMs and BMSCs was extracted using RIPA buffer (Pierce) while

maintained on ice. As for alveolar bone tissue around implants, the alveolar bone around the implant was first separated and then immersed in liquid nitrogen. The bone was then placed into a centrifuge tube containing grinding beads and ground to obtain a protein lysate. Following this, the samples were denatured at 95 ℃ for 10 minutes in SDS loading buffer and subsequently separated on 10% SDS–polyacrylamide gels (Beyotime). The separated proteins were then transferred onto polyvinylidene difluoride (PVDF, Millipore) membranes activated with methanol. After 5% BSA was applied to the membranes and allowed to incubate for 2 hours, the membranes were exposed to primary antibodies (listed in Supplementary Table 2) overnight at 4 ℃. The following day, the membranes were subjected to incubation with corresponding horseradish peroxidase (HRP)-conjugated secondary antibodies, followed by an additional incubation for 1–2 hours at 37 ℃. The detection of antibody-antigen complexes was achieved using gel imaging systems (Bio-Rad). The quantification of band densities was performed using ImageJ (National Institutes of Health) and subsequently normalized to the control.

**Osteogenic induction of BMSCs and ALP/ARS staining**

When BMSCs reached 70% confluency, culture medium was replaced with mineralization medium [growth medium supplemented with ascorbic acid (50μg/mL), b-glycerophosphate disodium (10 mM), and dexamethasone (100nM)].

As for ALP staining, after 7 days of osteogenic induction, cells were first fixed by 4% paraformaldehyde (Biosharp) for 15 min, and then stained with a BCIP/NBT Alkaline Phosphatase Color Development Kit (Beyotime) for 24 h.

As for ARS staining, after 14 days of osteogenic induction, cells were first fixed by 4%

paraformaldehyde (Biosharp) for 15 min, and then stained with Alizarin Red S solution (pH 4.2, Sigma) for 5 min.

**Senescence-associated β-galactose staining**

Cellular senescence was evaluated using senescence-associated β-galactosidase (SA-β-gal) staining kits (Beyotime). BMSCs were rinsed twice with PBS and subsequently fixed with a fixative solution for SA-β-gal staining for 15 minutes at room temperature. Then cells were washed three times with PBS and then incubated with the SA-β-gal staining solution at 37 °C for 24 h. The following day, cells were examined under an optical microscope.

**Enzyme-Linked immunosorbent assays (ELISA)**

The cell culture supernatant of BMDMs and BMSCs was harvested following the provided guidelines. The levels of IL-1β, TNF-α, and IL-6 in the supernatant were quantified utilizing ELISA kits (Elabscience).

**Flow cytometry**

To detect apoptosis level, BMSCs treated with P5091 for 3 days and *shUsp7* were prepared in staining buffer and stained with 1 μL FITC Annexin V and PI (APEBIO) for 30 minutes. After incubation, the cells were washed by PBS for 3 times. After the last wash and centrifugation, the cells were once again resuspended in staining buffer for analysis using Attune Nxt Flow Cytometer (Thermo Scientific).

As for efferocytosis and efferocytosis-induced M2 polarization, Jurkat cells (SCC-121815, Solarbio) were first labeled by DiIC18(5)-DS (MCE), then exposed to UV light (150 mJ/cm2) for 15 minutes with an open lid. Then apoptotic Jurkat cell were incubated with BMDMs for 24 h. After that, BMDMs were suspended in the staining buffer (BD Biosciences). To prevent

nonspecific binding, BMDMs were pre-incubated with FC block (BD Biosciences, 1:200) for 20 minutes. They were then incubated with either of the following antibodies on ice for 30 minutes: PE Rat Anti-Mouse F4/80 (BD Biosciences, 1:100) Alexa Fluor® 647 Rat Anti-Mouse CD206 (BD Biosciences, 1:50). After incubation, the cells underwent three washes with staining buffer and were subsequently resuspended in staining buffer. After the last wash and centrifugation, the cells were once again resuspended in staining buffer for analysis using Attune Nxt Flow Cytometer (Thermo Scientific). FACS data analysis was conducted using FLOWJO™ Software.

**Live/dead staining**

Calcein-AM (Beyotime) and 7-Aminoactinomycin D (7-AAD, Beyotime) were employed for concurrent fluorescence assessment. First, Calcein-AM (5 μM) was added into the culture medium for 30 min. Then, after cells were washed by PBS for 3 times, 7-AAD (5 μM) were added into the culture medium for 10 min. The distinction between living (green) and deceased (red) cells was ascertained using a fluorescence microscope and Image J software (National Institutes of Health) for cell quantification.

**Efferocytosis assay (Immunofluorescence staining)**

First, Jurkat cells (SCC-121815, Solarbio) were labeled with 5 μM Calcein-AM (Beyotime). Following a 2-hour incubation, Cells were washed for 3 times and subjected to UV irradiation (150 mJ/cm2) with an open lid. Subsequently, they underwent an additional 2-hour incubation before being introduced in a 1:1 ratio to BMDMs for 1 h. After 3 times of gentle washing, BMDMs were considered positive for phagocytosed green apoptotic Jurkat cells if they contained clusters of green dots measuring >3 μm in size. Quantification was performed

based on 3 images by Image J software (National Institutes of Health).

**Co-IP**

Treated BMDMs were lysed using Pierce IP Lysis Buffer (Thermo Fisher Scientific) following the provided instructions. Antibodies against USP7 (1:50, 31687, Cell Signaling Technology), EPSIN1 (1:100, ab86064, Abcam), HA (1:100, ab9110, Abcam; 1:100, M20013, Abmart), and Flag (1:100, ab205606, Abcam; 1:100, M20008, Abmart) were added to the lysates overnight at 4℃, and protein A/G beads were added into the mixture for another 4 h. After centrifugation, the pellet was collected and washed three times with lysis buffer. Subsequently, it was resuspended in RIPA buffer and boiled with SDS loading buffer at 95 ℃ for 10 minutes. The boiled samples were centrifuged again, and the supernatant was utilized for subsequent Western blot.

**In vivo experiments**

**Mice**

All animal experiments were approved by Subcommittee on Research and Animal Care (SRAC) of Sichuan University. Young (3-month-old) and aged (18-month-old) male wild-type C57BL/6J mice were purchased from Chengdu Dossy Experimental Animals Co. Ltd. The mice were housed in SPF facilities with a 12 h light/dark cycle and provided with sufficient food and water. A total of one hundred mice were used in this study. The sample size in different experiments was based on former studies and pre-experiments which was analyzed by One-way ANOVA F test. We randomized mice by body weight using the random function in EXCEl. The mice were randomly divided into 5 groups under double blindness: young mice treated with vehicle, young mice treated with P5091, aged mice treated with vehicle, aged

mice treated with P5091, and aged mice treated with P5091 and RAP. During experiment periods, no mice were excluded. USP7 inhibitor P5091 was dissolved in PBS containing 4% DMSO. Mice were injected daily i.p. with injections of vehicle (4% DMSO in PBS) or P5091 (5 mg/kg) or receptor-associated-protein (RAP, 20mg/kg) for 4 weeks based on former studies. All animal experiments described above were conducted in accordance with the ARRIVE guidelines.

**Implant surgery**

All mice were were anesthetized via intraperitoneal injection of ketamine at 80 mg/kg (Sigma Chemical) and xylazine at 10 mg/kg (Sigma Chemical). Following oral saline cleaning, a 2 mm incision was made anterior to the left first upper molars to mark the implant site. The implant site was prepared under saline cooling using a surgical motor (NSK-Nakanishi). Subsequently, the pilot hole was adjusted to accommodate the titanium implant (WEGO) using a drill. The titanium implant was then screwed into the implant bed with a screwdriver. Following the surgery, the mice were provided with a soft diet and were injected daily i.p. with injections of vehicle (4% DMSO in PBS) or P5091 (5 mg/kg) for 4 weeks.

**MicroCT**

The harvested femur and maxillary bones were first fixed in 4% paraformaldehyde for 24 h. Micro-CT analysis was carried out using the Hiscan XM Micro-CT system (Hiscan Information Technology Co., Ltd.), with a spatial resolution of 10 μm and utilized the following settings: 80 kV, 100 μA, and 50 ms integration time per step. As for femur, the region of interest (ROI) was defined as the region located 700 μm below the growth plate of the femur. Bone morphological parameters, including, bone volume per total volume (BV/TV), trabecular number (Tb.N), and

trabecular thickness (Tb.Th), cortical bone thickness (Ct.Th), and cortical bone area (Ct.Ar) were assessed within the ROI. As for the maxilla, the region of interest, composed of a radius of 200 μm around the implants, was selected for the reconstruction of alveolar bone, encompassing the central 50% portion of the implants. Parameters including BV/TV and bone-implant contact (BIC) were evaluated within this defined region.

**Histomorphometric/immunofluorescence staining analysis**

For histological analyses, the maxillary bones were initially fixed in 4% paraformaldehyde at 4 °C for 24h and subsequently transferred to PBS at 4 °C.

As for immunofluorescence staining and immunohistochemical staining, the maxillary bones were decalcification in EDTA (pH 7.2, Biosharp) for 6 weeks, allowing the bone to become pliable. The decalcified tissue were then embedded in paraffin, and 4-μm sections were obtained for subsequent staining.

As for immunofluorescence staining, the following primary antibodies and fluorescent dyes were utilized in this study: anti-F4/80 (Abcam, ab6640, 1:100), DAPI (Beyotime), and TUNEL (Beyotime). The detection of the primary antibodies was carried out using the corresponding Alexa Fluor-conjugated secondary antibodies (Abcam). All tissue sections were examined under a fluorescent microscope (Leica).

As for immunohistochemical staining, the sections were stained by ALP antibody (ET1609-68, Huabio) and USP7 antibody (A300-033A, ThermoFisher). The positive-expression area of ALP wa calculated by IHC plugins in imageJ (National Institutes of Health). The ratio of ALP-positive area was calculated by the pixels of positive-expression area of ALP and the pixels of whole bone tissue in images. TRAP staining was performed according to the

instructions provided in the Beyotime TRAP Staining Kit (P0332). The number of osteoclasts was calculated by imageJ (National Institutes of Health).

**Statistical analysis**

Statistical analyses were conducted using GraphPad Prism version 8.0 and SPSS 22.0 software. The data are expressed as means with standard deviation (SD). The normality of data was first verified by Shapiro–Wilk test. Two-tail student's t-test was employed to compare two groups, while one-way analysis of variance (ANOVA) was applied when analyzing three or more than three groups. For multiple comparisons, the Bonferroni's multiple comparisons test was utilized. Sample sizes are specified in the figure legends. Statistical significance was defined as *$P$< 0.05, **$P$ < 0.01, ***$P$ < 0.001, and ****$P$ < 0.0001.

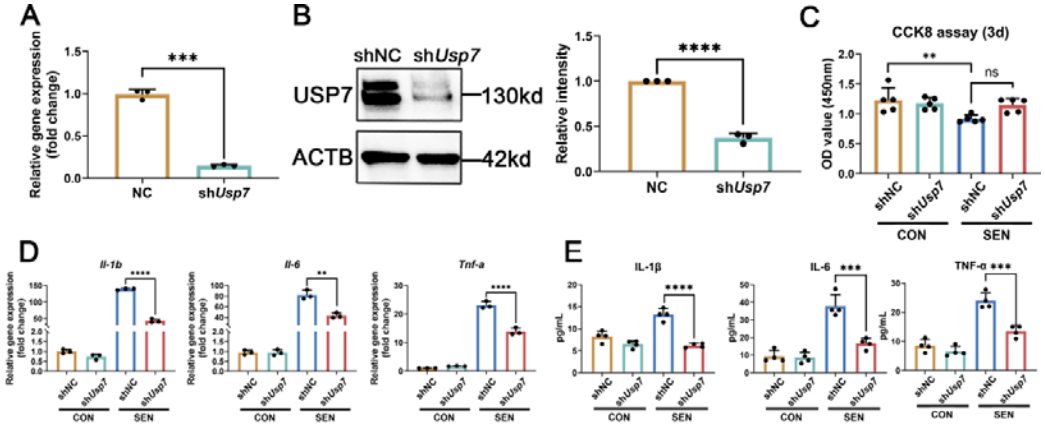


**Appendix Figure 1.** Generation of USP7-depleted BMDMs and USP7 depletion inhibited innate immune response. (A) qPCR showing downregulated mRNA level of USP7 in BMDMs transfected with sh*Usp7*, n = 3. (B) WB analysis showing downregulated protein level of USP7 in BMDMs transfected with sh*Usp7*, n = 3. (C) CCK8 assay determining cell viability of control/senescent BMDMs at 3d after transfected with sh*Usp7*, n = 5. (D) qPCR results of

*IL-1b, IL-6*, and *Tnf-a* mRNA expression in different groups of BMDMs, n = 3. (E) ELISA results of IL-1β, IL-6, and TNF-α secretion level in different groups of BMDMs, n = 4. shNC, BMDMs transfected with NC lentivirus; shUsp7, BMDMs transfected with shUsp7 lentivirus; CON, control BMDMs; SEN, senescent BMDMs. Data are shown as the mean ± SD; ns, not significant, **P* < 0.05, ***P* < 0.01, ****P* < 0.001, *****P* < 0.0001.

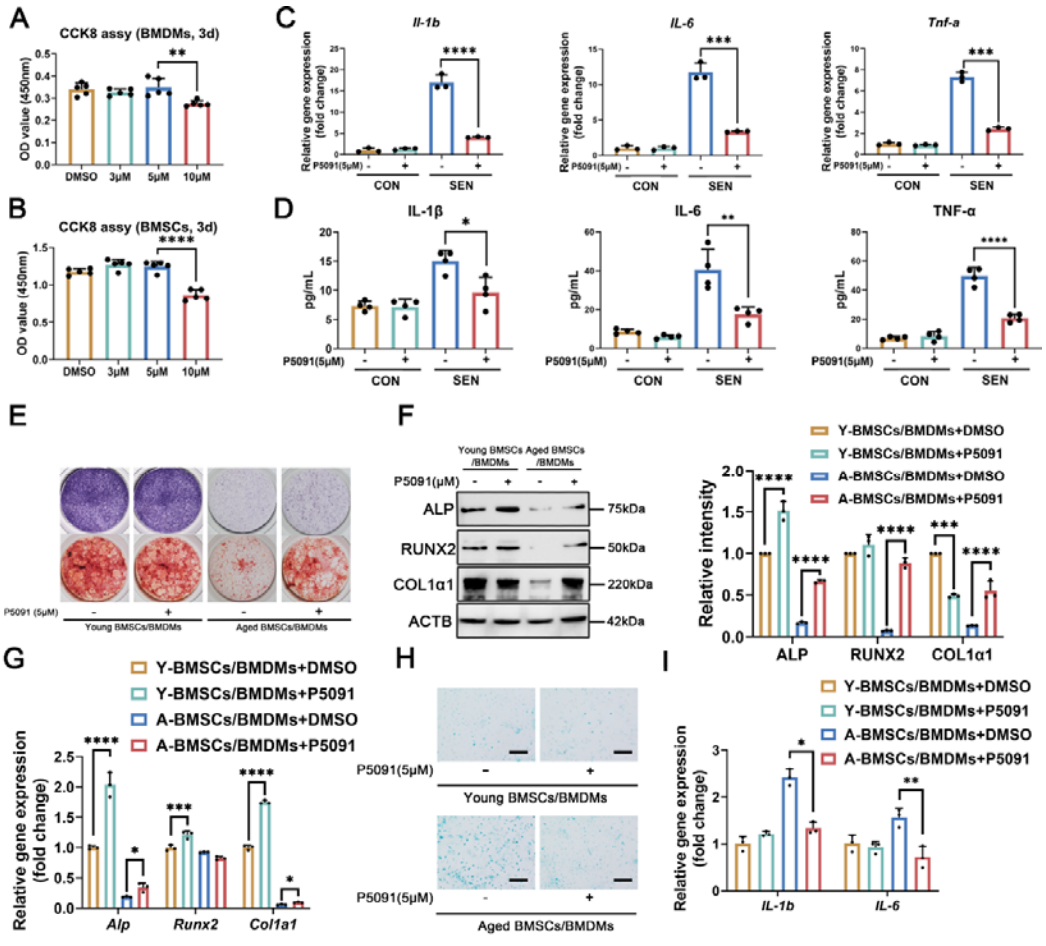


**Appendix Figure 2.** P5091 inhibited inflammation in senescent BMDMs and promoted osteogenesis of aged BMSCs co-cultured with BMDMs. CCK8 demonstrating the changes in cell viability of BMDMs (A) and BMSCs (B) in response to varying concentrations of P5091 at 3d, n = 5. (C) qPCR results of the mRNA levels of *IL-1b*, *Tnf-a*, and *IL-6* in different groups of

BMDMs treated P5091, n = 3. (D) ELISA results of IL-1β, IL-6, and TNF-α secretion level in different groups of BMDMs treated with P5091, n = 4. (E) Representative images of ALP/ARS staining of BMSCs co-cultured with BMDMs. (F) WB results and quantification of the protein level of ALP, RUNX2, and COL1α1 in BMSCs co-cultured with BMDMs, n = 3. Y-BMSCs, young BMSCs; A-BMSCs, aged BMSCs; shNC, BMDMs transfected with shNC lentivirus; shUsp7, BMDMs transfected with shUsp7 lentivirus; CON, control BMDMs; SEN, senescence BMDMs. Data are shown as the mean ± SD; ns, not significant, *$P < 0.05$, **$P < 0.01$, ***$P < 0.001$, ****$P < 0.0001$.

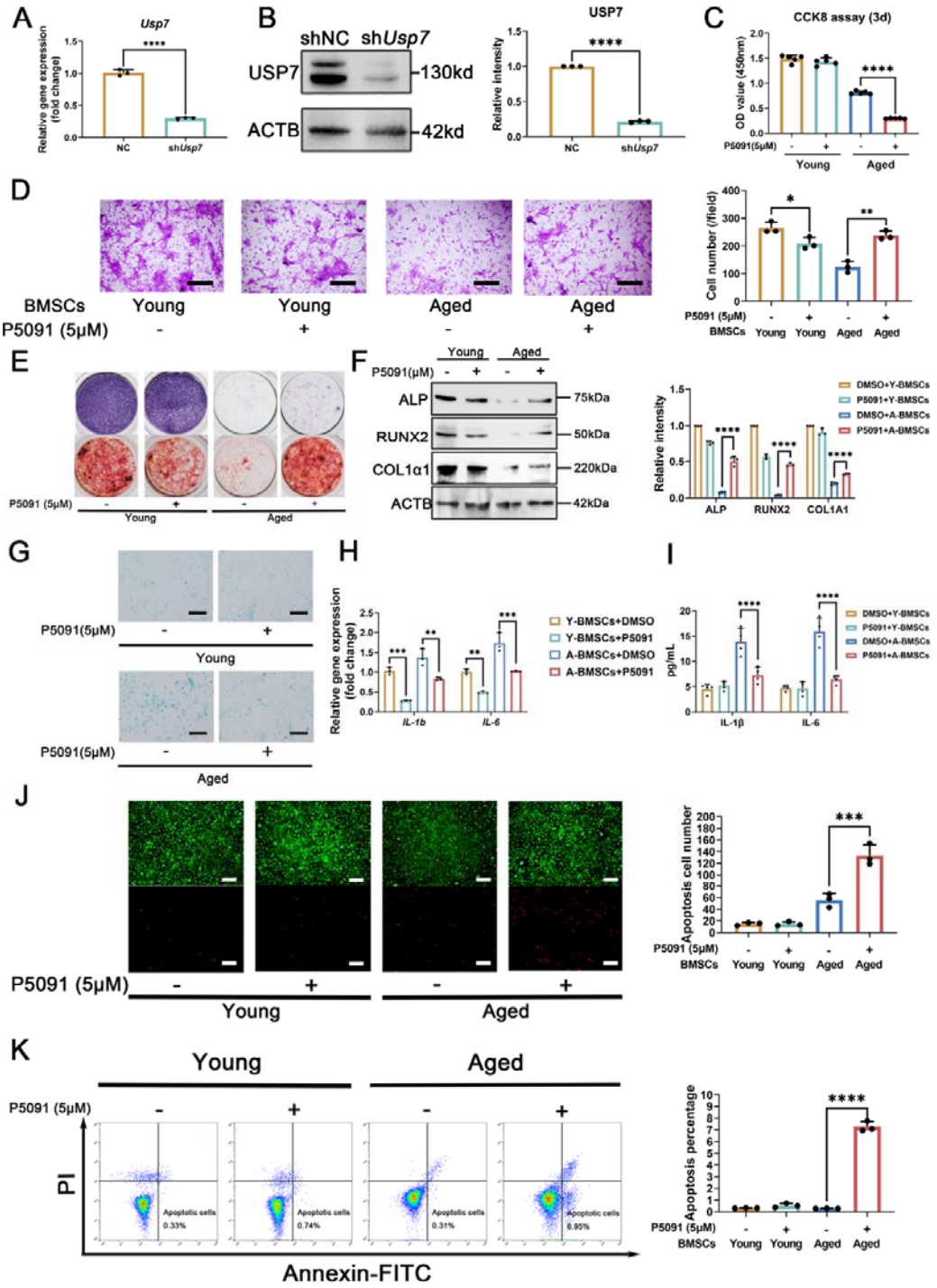


**Appendix Figure 3.** Generation of USP7-depleted BMSCs and P5091 promoted osteogenesis and senolysis in aged mice. (A) qPCR showing downregulated mRNA level of USP7 in BMSCs transfected with sh*Usp7*, n = 3. (B) WB analysis showing of downregulated

protein level of USP7 in BMSCs transfected with sh*Usp7*, n = 3. (C) CCK8 assay determining decreased cell viability in aged BMSCs treated with P5091 at 3d, n = 5. (D) Transwell assay indicating that P5091 promoted cell migration in aged BMSCs, n = 3. (E) Representative images of ALP/ARS staining showing that P5091 altered osteogenic capacity in young and aged BMSCs. (F) WB results and quantification determining that altered protein level of ALP, RUNX2, and COL1α1 in young and aged BMSCs treated with P5091 at 7d, n = 3. (G) Representative images of SA-β-gal staining of different groups of BMSCs with P5091, scale bar, 50μM. (H) qPCR results showing that mRNA level of *IL-1b* and *IL-6* in different groups of BMSCs with P5091 at 3d, n = 3. (I) ELISA results showing that secretion level of IL-1β and IL-6 in different groups of BMSCs with P5091 at 3d, n = 4. (J) Representative images and quantitative analysis of live/dead staining of BMSCs after treated with P5091s for 3d, green color indicates live cells, red color indicates dead cells, scale bar, 150μm, n = 3. (K) Flow cytometry and quantitative analysis for apoptosis in BMSCs after treated with P5091 for 3d, n = 3. shNC, BMSCs transfected with NC lentivirus; sh*Usp7*, BMSCs transfected with shUsp7 lentivirus; young, young BMSCs; aged, aged BMSCs. Data are shown as the mean ± SD; ns, not significant, *$P < 0.05$, **$P < 0.01$, ***$P < 0.001$, ****$P < 0.0001$.

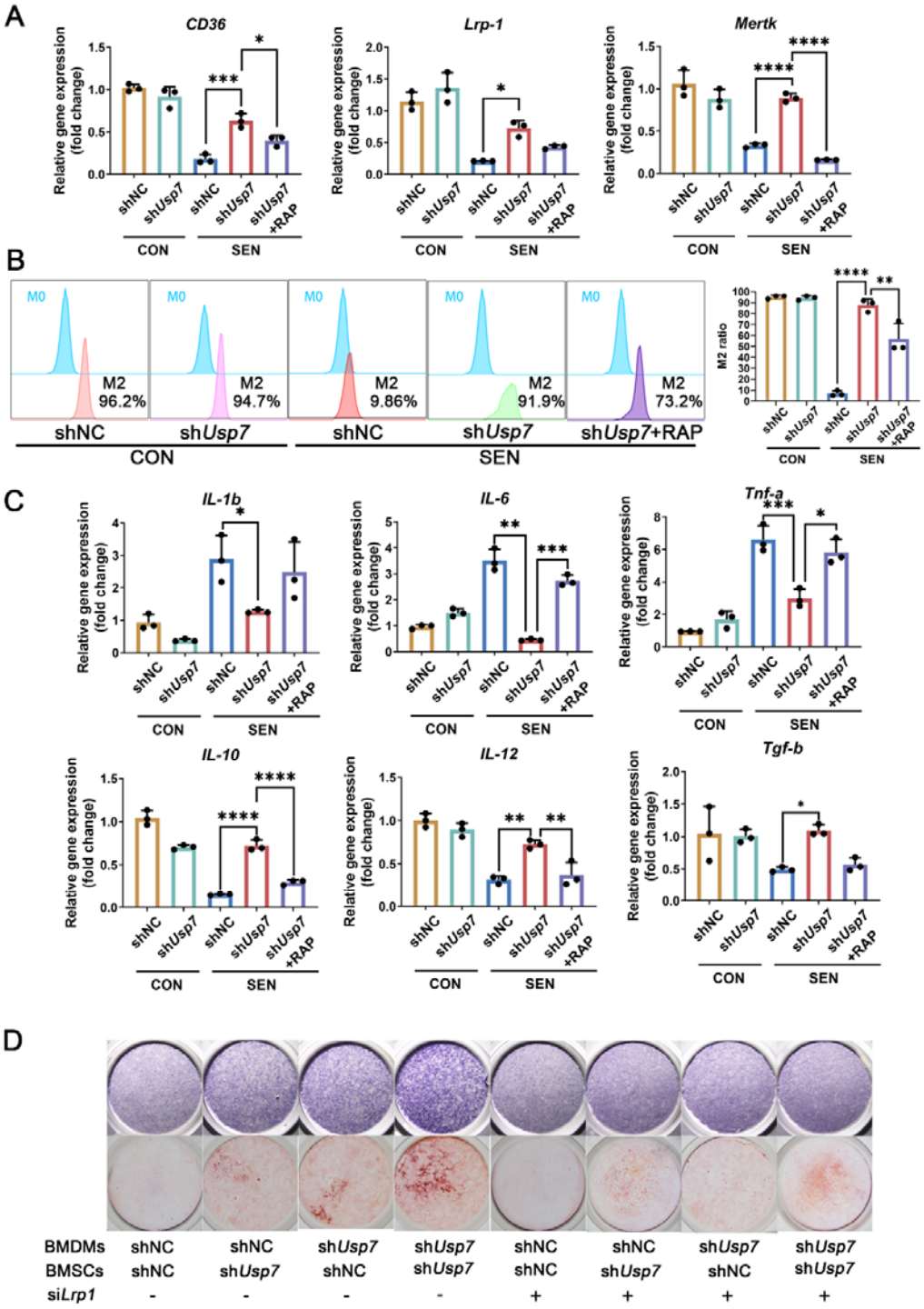


**Appendix Figure 4.** USP7 depletion improved pro-osteogenic capacity and inhibited inflammation in senescent BMDMs engulfing apoptotic cells. (A) qPCR results showing mRNA level of efferocytosis-related genes (*CD36, Lrp1,* and *Mertk*) in BMDMs, n = 3. (B) Flow

cytometry showing M2 polarization in different groups of BMDMs that engulfed apoptotic Jurkat cells, n = 3. (C) qPCR results showing mRNA level of pro-inflammatory-related genes (IL-1b, IL-6, and *Tnf-a*) and anti-inflammatory-related genes (*IL-10, IL-12,* and *Tgf-b*) in different groups of BMDMs, n = 3. (D) Representative images of ALP/ARS staining of BMSCs co-cultured BMDMs directly. shNC, BMDMs transfected with NC lentivirus; shUsp7, BMDMs transfected with shUsp7 lentivirus; CON, control BMDMs; SEN, senescence BMDMs; RAP, receptor-associated-protein. Data are shown as the mean ± SD; ns, not significant, *$P < 0.05$, **$P < 0.01$, ***$P < 0.001$, ****$P < 0.0001$.

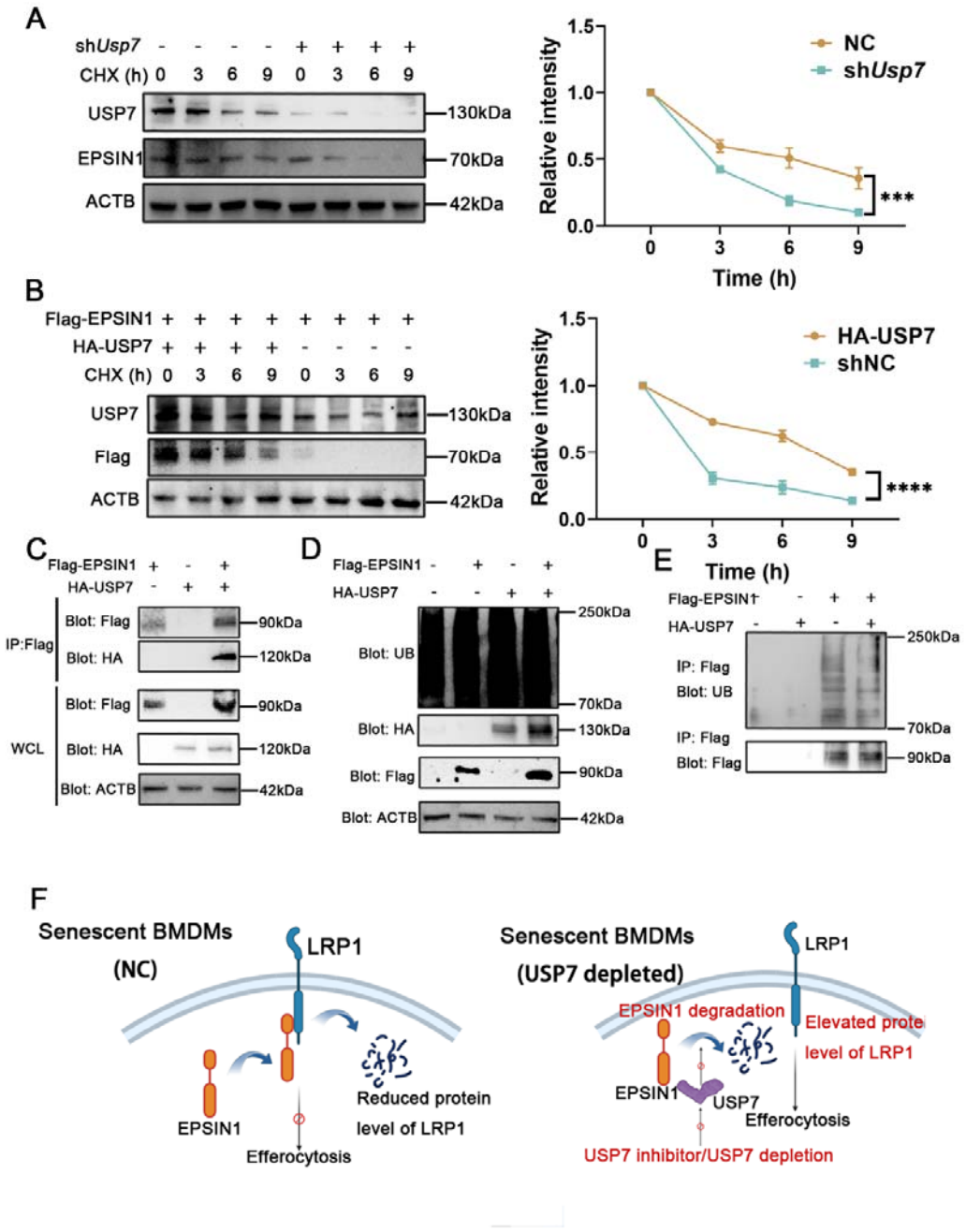


**Appendix Figure 5.** USP7 regulated LRP1-mediated efferocytosis by deubiquitinating EPSIN1. (A) WB results showing the time-dependent expression of EPSIN1 in USP7-depleted BMDMs, n = 3. (B) WB results showing the time-dependent expression of EPSIN1 in BMDMs

transfected with HA-USP7, n = 3. (C) Co-IP showing that the interaction between Flag-EPINS1 and HA-USP7 in different groups of BMDMs. (D) WB results showing the overall ubiquitous level in different groups of BMDMs. (E) Co-IP indicating that HA-USP7 over expression downregulated ubiquitous level of EPSIN1. (F) Schematic diagram showing that USP7 regulated LRP1-mediated efferocytosis by deubiquitinating EPSIN1. CHX, cycloheximide; IP, immunoprecipitation; WCL, whole cell lysate. Data are shown as the mean ± SD; ns, not significant, ***$P < 0.001$, ****$P < 0.0001$.

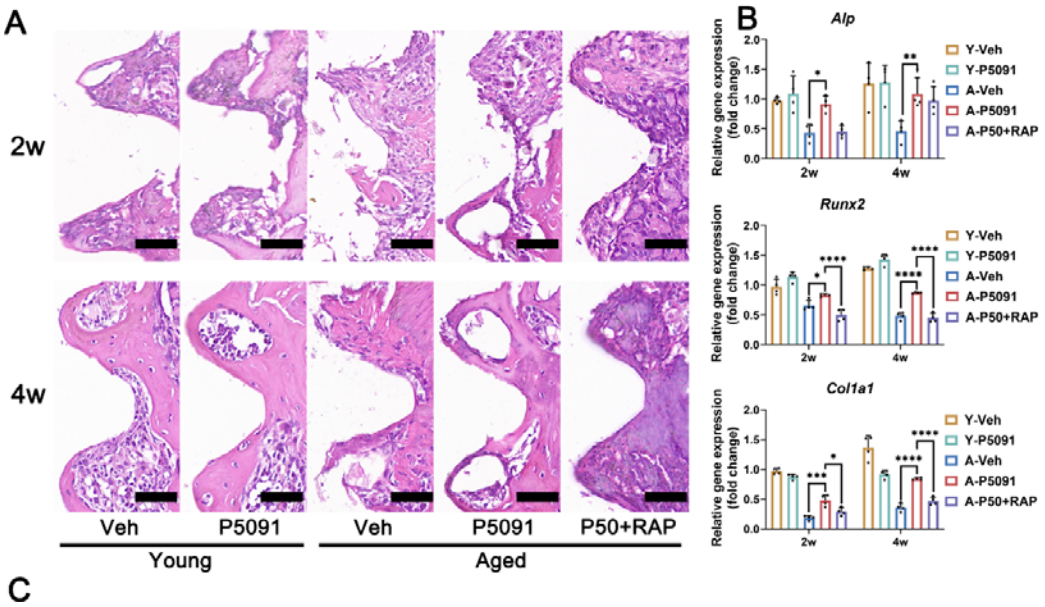


C

**Appendix Figure 6.** P5091 promoted osteogenesis in peri-implant bone tissue of senile osteoporotic mice. (A) HE staining of peri-implant bone tissue at 2-week and 4-week in different groups of mice. (B) qPCR results showing that mRNA level of *Alp, Runx2,* and *Col1a1* in peri-implant bone tissue of different groups of mice, n = 3. Veh, vehicle; RAP, receptor-associated-protein; Young, young mice; Aged, senile osteoporotic mice. Data are shown as the mean ± SD; ns, not significant, *$P < 0.05$, **$P < 0.01$, ***$P < 0.001$, ****$P <$

0.0001.

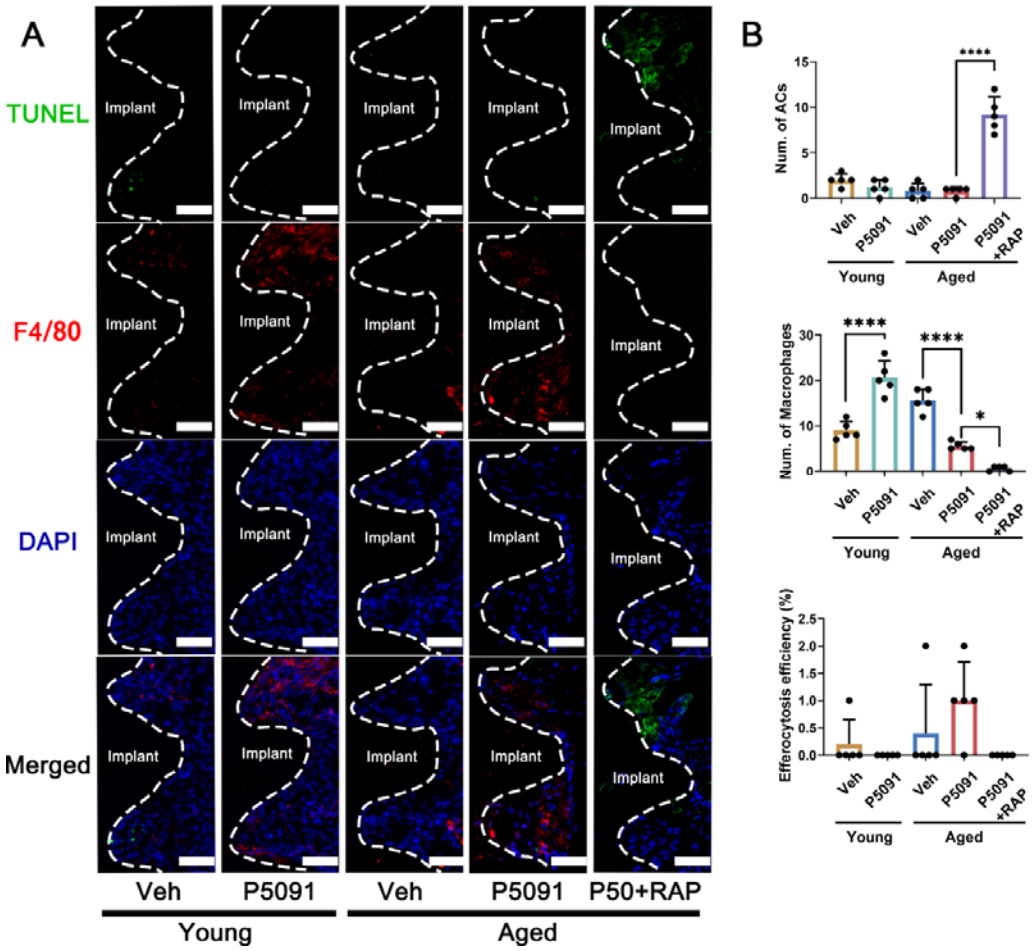


**Appendix Figure 7.** P5091 did not alter efferocytosis at 4-week of osseointegration. (A) Representative immunofluorescence images of macrophages and apoptotic cells around the implants, scale bar, 60μM. Veh, vehicle; RAP, receptor-associated-protein; Young, young mice; Aged, senile osteoporotic mice. Data are shown as the mean ± SD; ns, not significant, *$P$ < 0.05, **$P$ < 0.01, ***$P$ < 0.001, ****$P$ < 0.0001.

**Appendix Table 1.** Primers sequences used in this research.

| Targets (mouse) | Primer Sequence |
|---|---|

| | |
|---|---|
| *β-actin F* | CATCCGTAAAGACCTCTAGCCAAC |
| *β-actin R* | ATGGAGCCACCGATCCACA |
| *Alp F* | AACCCAGACACAAGCATTC |
| *Alp R* | GCCTTTGAGGTTTTTGGTCA |
| *Runx2 F* | GGTACTTCGTCAGCATCCTATCAG |
| *Runx2 R* | GCTTCCGTCAGCGTCAACAC |
| *Col1α1 F* | GCTTCACCTACAGCACCCTTGT |
| *Col1α1 R* | TGACTGTCTTGCCCCAAGTTC |
| *Il-1β F* | ACCCCAAAAGATGAAGGGCT |
| *Il-1β R* | GATACTGCCTGCCTGAAGCTCT |
| *Il-6 F* | TAGTCCTTCCTACCCCAATTTCC |
| *Il-6 R* | TTGGTCCTTAGCCACTCCTTC |
| *Tnf-a F* | CCCTCACACTCAGATCATCTTCT |
| *Tnf-a R* | GCTACGACGTGGGCTACAG |
| *p53 F* | CTCTCCCCCGCAAAAGAAAAA |
| *p53 R* | CGGAACATCTCGAAGCGTTTA |
| *CD36 F* | ATGGGCTGTGATCGGAACTG |
| *CD36 R* | GTCTTCCCAATAAGCATGTCTCC |

| | |
|---|---|
| *Lrp1 F* | ACTATGGATGCCCCTAAAACTTG |
| *Lrp1 R* | GCAATCTCTTTCACCGTCACA |
| *Mertk F* | CAGGGCCTTTACCAGGGAGA |
| *Mertk R* | TGTGTGCTGGATGTGATCTTC |
| *IL-10 F* | GCTCTTACTGACTGGCATGAG |
| *IL-10 R* | CGCAGCTCTAGGAGCATGTG |
| *Tgf-b F* | CTCCCGTGGCTTCTAGTGC |
| *Tgf-b R* | GCCTTAGTTTGGACAGGATCTG |
| *IL-12 F* | CCTGGCTCTTGCTTGCCTT |
| *IL-12 R* | GGTCTTGTGTGATGTTGCTCA |

**Appendix Table 2.** Antibodies used in this research.

| Antibody | Source | Host | Dilution |
|---|---|---|---|
| p16INK4a | Abcam, ab211542 | Rabbit | 1:100 |
| NLRP3 | Adipogen, AB_2490202 | Mouse | 1:1000 |
| cleaved IL-1β | Cell Signaling Technology, Asp116 | Rabbit | 1:1000 |
| cleaved | Adipogen, AG-20B-0042-C100 | Mouse | 1:1000 |

| | | | |
|---|---|---|---|
| caspase-1(p20) | | | |
| GSDMD | Huabio, HA601046 | Mouse | 1:1000 |
| GSDMD-NT | | | |
| β-actin | Huabio, EM21002 | Mouse | 1:1000 |
| ALP | Huabio, ET1609-68 | Rabbit | 1:500 |
| RUNX2 | Huabio, ET161247 | Rabbit | 1:500 |
| COL1α1 | SAB, 28307 | Rabbit | 1:500 |
| USP7 | ThermoFisher, A300-033A | Rabbit | 1:50 |
| EPSIN1 | Abcam, ab75879 | Rabbit | 1:100 |
| LRP1 | Abcam, ab92544 | Rabbit | 1:100 |
| Rabbit Anti-HA | Abcam, ab9110 | Rabbit | 1:100 |
| Rabbit Anti-Flag | Abcam, ab1162 | Rabbit | 1:100 |
| Mouse Anti-HA | Abmart, M20003 | Mouse | 1:100 |
| Mouse Anti-Flag | Abmart, M20008 | Mouse | 1:100 |

| | | | |
|---|---|---|---|
| HRP Goat Anti-Rabbit IgG (H+L) | Huabio, HA710308 | Goat | 1:10000 |
| HRP Goat Anti-Mouse IgG (H+L) | Huabio, HA710142 | Goat | 1:10000 |
| F4/80 | Abcam, ab6640 | Mouse | 1:100 |